Batteries & Supercaps

Research Article
doi.org/10.1002/batt.202300452

Chemistry Europe
European Chemical Societies Publishing

www.batteries-supercaps.org

Unveiling Oxygen Evolution Reaction on $LiCoO_2$ Cathode: Insights for the Development of High-Performance Aqueous Lithium-ion Batteries

Gibu George,[a] Albert Poater,[a] Miquel Solà,[a] and Sergio Posada-Pérez*[a]

Aqueous lithium-ion batteries (ALIBs) are attracting significant attention as promising candidates for safe and sustainable energy storage systems. This paper delves into the crucial aspects of ALIB technology focusing on the interaction between $LiCoO_2$ (lithium cobalt oxide) cathode material and water electrolytes, with a specific emphasis on the Oxygen Evolution Reaction (OER) process. Fundamental understanding of the electrochemical behavior of $LiCoO_2$ in aqueous electrolytes is crucial for enhancing the performance, safety, and longevity of ALIBs using $LiCoO_2$ as the cathode material.

Through a comprehensive periodic density functional analysis of the $LiCoO_2$-water at the cathode interface, the potential catalytic contributions to the OER mechanism of $LiCoO_2$ are explored. The catalytic properties of $LiCoO_2$ towards OER are investigated considering different steady states of the lowest energy surfaces of $LiCoO_2$ and three different Li concentrations. Our results do not predict the formation of oxygen gas due to the expected large overpotentials, although the exergonic water decomposition to hydroxyl by means the first proton-electron transfer is predicted at equilibrium potential. This work contributes to the fundamental understanding of $LiCoO_2$ as cathode for aqueous lithium-ion batteries, reporting the pros and cons of one of the most common cathode materials for traditional non-aqueous batteries.

Introduction

In 1980, John Goodenough improved the work of Stanley Whittingham discovering the high energy density of lithium cobalt oxide ($LiCoO_2$), doubling the capacity of then-existing lithium-ion batteries (LIBs).[1] $LiCoO_2$ (LCO) offers high conductivity and large stability throughout cycling with 0.5 Li^+ per formula unit ($Li_{0.5}CoO_2$). The reason behind this amazing performance is its high electronic conductivity, since the delithiation process implies a change in its semiconductor behavior ($LiCoO_2$) to the metallic one ($Li_{0.9}CoO_2$) favoring the (de)intercalation of Li^+ ions.[2] The first prototype of Li-ion battery was patented by Yoshino[3] and was composed by an organic electrolyte using $LiCoO_2$ as the positive electrode and a carbonaceous material as the negative electrode material, since their capability to (de)intercalate Li^+ ions was proved by Yazami and Touzain.[4]

For more than three decades, LIBs have been powering most of our portable devices, nowadays essential to the pace of life in today's society, and they will be crucial to renew the fleet of fuel and diesel cars to electric ones. Although LIBs are a very mature technology, it is currently too expensive for large-scale storage. A very attractiveness alternative to reduce the cost of LIBs is to replace the traditional organic electrolytes by water.[5,6] Organic electrolytes, a usually flammable organic solvents, present the main advantage that they can operate at very high voltages, 3 to 4 V,[7] due to the high electrochemical stability. In contrast, they have poor thermal stability, which leads to the electrolyte decomposition or violent chemical reactions and their fabrication implies high cost due to the complex preparation. An interesting and low-cost[8] alternative to elude the safety problems is the use of aqueous electrolytes.[9–15] Despite the most common drawbacks of aqueous batteries, like possible proton intercalation[16,17] or limited energy density performance due to the shorter voltage stability window, 1.23 V,[18,19] the non-flammability and low fabrication cost is a great advantage over organic liquid electrolytes.[20]

Regarding the rising star cathode material, LCO has been extensively studied for batteries that uses organic electrolytes.[21–25] However, the number of articles reporting the performance of LCO as cathode for aqueous electrolytes is scarce. The research in water electrolytes has been focused on the reversible lithium intercalation reactions to store and release energy efficiently. Some of these studies investigated the thermochemical stability of LCO and the possible proton by Li^+ exchange, reporting the large stability of the protonated material and the irreversible Li deintercalation.[16,26] Nevertheless, thermodynamic analysis performed by means of density functional theory (DFT) calculations proved that this cation exchange and proton intercalation process is not feasible at

[a] G. George, Dr. A. Poater, Prof. Dr. M. Solà, Dr. S. Posada-Pérez
Institut de Química Computacional i Catàlisi and Departament de Química
Universitat de Girona
c/Maria Aurèlia Capmany 69, 17003 Girona, Catalonia (Spain)
E-mail: sergio.posada@udg.edu

Supporting information for this article is available on the WWW under https://doi.org/10.1002/batt.202300452

battery operation conditions.[27] Other experimental studies explored the electrochemical performance of LCO as a cathode material for reversible Li intercalation using a highly concentrated lithium nitrate and lithium sulphate aqueous solutions,[28–30] revealing that LCO showed the same pattern observed using non-aqueous electrolytes with very low degradation, mainly related with surface effects due to vacancy[31] and defects generation. The formation of lithium hydroxide and cobalt hydroxide on the surface of the material is one of the common drawbacks to use LCO as the cathode for aqueous LIBs (ALiBs), since these hydroxides can compromise the performance of the cathode. However, during the reverse Li intercalation reaction, only the formation of Co_3O_4 spinel planes were detected at surface level, without a decay in the battery performance.[31] Furthermore, it was reported that the use of additives helps to stabilize LCO at high voltages.[32]

Although some DFT studies explored the stability of LCO surfaces in water environment,[33,34] the mechanism of interaction and bonding between LCO surface and water has not been deeply studied, specially at atomistic framework, as well as the possible water decomposition to produce oxygen (oxygen evolution reaction, OER). This reaction is undesired since the formation of oxygen gas can cause pressure buildup and lead to potential safety concerns for the battery. The OER is known to be a relatively sluggish reaction that requires an overpotential (voltage above the thermodynamic equilibrium potential) to be produced. Thus, the selected cathode should have high operating voltage and energy density, rapid charge and discharge rates, resist the possible water degradation, and to be a bad electro-catalyst for OER.

In this work, we use DFT simulations to investigate the OER on the most stable surfaces of the LCO cathode material. Our work not only evaluates the binding energies of the widely accepted four electron-proton transfer mechanism, but also analyzes the role of lattice oxygen and oxygen vacancy formations on the catalytic pathway of OER. Understanding the interplay between LCO and aqueous electrolytes, particularly the interaction with water molecules and its activity towards the OER is essential in the strategic advancement of new generation of aqueous ion batteries, fostering the evolution of this green energy storage technology.

Computational Details and Surface Models

All calculations have been carried out with the Viena Ab Initio Package code (VASP).[35] The periodic simulations have been performed using the Perdew-Burke-Ernzerhof (PBE) exchange-correlation functional[36] including an effective *U* value following the Dudarev approach[37] to better describe the local character of the strongly correlated 3*d* electrons of the Co atoms. For sake of consistency and better comparison with previous results, we have adopted the computational scheme available in Materials Project Database[38] for $LiCoO_2$ using a *U* value of 3.2 eV. All computations have been designed considering the Co atoms in a high-spin ferromagnetic state, although the spin relaxation is allowed.[38] The effects of the core electrons on the valence ones have been taken into account by means of the projected augmented wave (PAW) method of Blöchl[39] as implemented by Joubert.[40] A Monkhorst–Pack grid of 5×5×1 k-points was used for the integration in the reciprocal space of all surfaces[41] following the same scheme used for the same surfaces terminations in the previous study.[42] For the atomic relaxation, the convergence has been achieved when the forces of the atoms were smaller than 0.01 eV $Å^{-1}$.

The surface terminations of LCO employed in this study have been selected according previous DFT studies.[42–45] Thus, the polar (001) and (012) terminations and the non-polar (104) and (110) surfaces have been used. The polar (001) and non-polar (104) surfaces are the most stable, as also found in experiments. Nevertheless, this surface stability is accounted considering the stoichiometric configurations at standard conditions. It should be borne in mind that during battery operation Li atoms are (de)intercalated, and the surface energy is sensitive to the Li chemical potential μ_{Li}.[42,43] We have modeled the four surface terminations considering eight $LiCoO_2$ formula units so that the corresponding supercells contain 8 Co and 16 O atoms as it was performed in the previous study.[42] On both non-polar surfaces, (104) and (110) terminations, all three species, Li, Co, and O, are distributed in each layer in a stoichiometric ratio. The slab models contain four layers (see Figure S1). The two half-top atomic layers have been relaxed during the optimization process. In contrast, for the polar surfaces, (001) and (012) terminations, a reconstruction was required to redistribute the charge of the slabs.[46] The (001) surface originally contains 8 layers following the Li–O–Co–O pattern repeated twice, since Li terminated is the lowest in energy. To avoid the creation of an infinite electric field, the surface has been reconstructed moving half of the Li monolayer on the top to the bottom of the surface. Therefore, the slab models contain 9 layers, with the top 4.5 layers relaxed and the bottom 4.5 frozen. For (012) termination, 9 layers are used as well, being the top and the bottom layers of the slab half of the O monolayer. However, the thickness is lower than the (001) since the Li–Co and O layers are very close. Further details, see supporting information and the previous DFT studies.[42,43] Finally, to mimic the different steady states of the surfaces during the battery operations, different concentrations of Li atoms have been considered to further explore the O_2 generation at different stages of the charge/discharge process. The slab models with less Li content have been constructed removing the most external Li atoms of the most external layers and allowing the displacement of the half-top atoms of the slab. The surface energy and the voltage at which the delithiation process occurs is calculated according to the following equation 1:

$$V = -\frac{\mu_A^{\text{cathode}} - \mu_A^{\text{anode}}}{zF} = -\frac{\mu_A - \mu_A^{\text{ref}}}{zF} \quad (1)$$

where *z* is the transferred charge, *F* is the Faraday constant, and A represents Li^+. Scanning the possible values for μ_{Li}, one can explore the surface stability with respect to Li^+/Li voltage.

The reaction mechanism of OER considered in this work encompasses four elementary steps [Equations (2)–(5)],[47,48] where the water molecule evolves to hydroxyl moieties, which decomposes to atomic oxygen. The dissociation of a second water molecule implies the formation of OOH species as a previous step of O_2 generation.

$$H_2O\ (l) + {}^* \rightarrow {}^*OH + H^+ + e^- \quad (2)$$

$$^*OH \rightarrow {}^*O + H^+ + e^- \quad (3)$$

$$H_2O\ (l) + {}^*O \rightarrow {}^*OOH + H^+ + e^- \quad (4)$$

$$^*OOH \rightarrow O_2 + {}^* + H^+ + e^- \quad (5)$$

Research Article
doi.org/10.1002/batt.202300452
Chemistry Europe
European Chemical Societies Publishing

The * represents the bare surface of full and partially delithiated $LiCoO_2$ and *OH, *O, and *OOH represents the Gibbs energy of the moieties adsorbed on the surfaces. Nevertheless, this reaction mechanism does not consider the possible effect of oxygen lattice of the catalysts as it has been reported in previous works, showing even more energetically favored pathway for OER in other metal oxides.[49–52] The most accepted mechanism, known as lattice oxygen evolution reaction (LOER) mechanism, is illustrated in Equations (6)–(9):

$$H_2O\ (l) + O_{lat} \rightarrow^{*} OH{-}O_{lat} + H^+ + e^- \quad (6)$$

$$^{*}OH{-}O_{lat} \rightarrow O_{vac} + O_2 + H^+ + e^- \quad (7)$$

$$O_{vac} + H_2O\ (l) \rightarrow^{*} H{-}O_{lat} + H^+ + e^- \quad (8)$$

$$^{*}H{-}O_{lat} + \rightarrow O_{lat} + H^+ + e^- \quad (9)$$

where O_{lat} is one of the lattice oxygens of LCO surfaces, *X–O_{lat} represent *OH and *H species adsorbed on O_{lat}, and O_{vac} represents the Gibbs energy of the surface with one oxygen vacancy. Some controversial points must be clarified. First of all, the first reaction step of both mechanisms (Reactions 2 and 6) will be the same if the *OH is bonded to one of the oxygens of the surface. It is often assumed that *OH is anchored to the metal atom of the metal oxide instead of one of the oxygens in the concerted mechanism. Nevertheless, if the adsorption on oxygen site is the lowest in energy, both steps are equivalent. It has been carefully detailed for each mechanism on the results section. On the other hand, the role of lattice oxygen can be evaluated on the concerted mechanism after the second proton-electron transfer, since the adsorption of *O species on top of the O_{lat} may imply the desorption of O_2, generating and oxygen vacancy on the material. All mechanisms have been investigated in this work.

The energy of $H^+ + e^-$ is computed as half of the Gibbs energy of the H_2 molecule at 0 V vs. standard hydrogen electrode (SHE) at 1 bar and 1 M activity following the Computational Hydrogen Electrode (CHE) approach proposed by Norskov and coworkers.[53] The reaction Gibbs energy of each step is computed considering the DFT energy of the adsorbed species including the zero-point energy correction and the entropic effects by means of the computation of the adsorbate frequencies (see SI for more details). As an example, the reaction Gibbs energy of step 3 is computed as $\Delta G_3 = \Delta G_{*O} + 1/2\ \Delta G_{H2} - \Delta G_{*OH} - eU_{SHE}$. According to CHE approach, to make the process feasible, the Gibbs energy of each reaction step must be exergonic, therefore the process must not have a thermodynamic energy barrier. In the case of endergonic process, i.e., where the following reaction intermediate is higher in energy with respect to the previous one, the U_{SHE} parameter is used to determine at which potential the process is energetically favored, known as the reaction limiting potential (see Figure S2 and Supporting Information for further details). The highest potential required for all the elementary steps is the limiting potential of the reaction process, and its difference with respect to the equilibrium potential (1.23 V) is known as the overpotential required to make the process feasible. Finally, it is important to clarify that these are thermodynamic equilibrium voltage either for intercalation/deintercalation process or OER steps, without considering experimental overpotentials observed during battery operation conditions.

Results and Discussion

For both mechanisms, with and without involving the oxygen lattice, the binding energy of the water molecule with the surface is not considered in the electrochemical reaction pathway. However, to investigate the interaction of water molecules with the cathode material is a pertinent step to elucidate the suitability of the cathode material to work with aqueous electrolytes. As collected in Table 1, the binding energy of water on the full lithiated (001) surface is 0.22 eV, showing slightly repulsive interaction. This is not unexpected since previous experimental studies revealed that the water-LCO becomes more favored when vacancies and defects are generated on the LCO lattice.[54,55] As a proof of fact, the binding energy of water molecule on partially delithiated surfaces becomes negative with values ranging from −0.80 to −1.60 eV. The huge difference observed in the binding energy is related to the adsorption site. The absence of Li on the most exposed surface layer allows the water adsorption with both H atoms pointing out oxygen surface atoms, generating H-bonds and moderate binding energies. The presence of oxygen vacancies on the lattice slightly varies the adsorption geometry, with only one of the hydrogen atoms in direct contact with the surface. For the (104) termination, large repulsive energies are reported in Table 1. The adsorption geometry has the oxygen atom on top of Co atom with the two hydrogens pointing to the oxygen surface atoms. The only favored interaction is found for the half-delithiated surface with oxygen vacancies. The unexpected fact is that the adsorption geometry is the same than the adsorption geometry for the rest of studied (104) configurations where positive binding energies have been reported (see Table 1). For (110) termination, the adsorption energy on full lithiated configuration is 0.66 eV and becomes isoenergetic with respect to the gas phase water molecule for partially delithiated systems. For full lithiated configuration, the oxygen of water is linked to one of the most external Li atoms while only one of the hydrogens is bonded to one of the oxygen atoms. However, the partially delithiated surfaces show both hydrogen atoms pointing out oxygen atoms on the surface, as it was observed for other LCO terminations. The same tendency has been observed for (012) surfaces, where the oxygen of water molecule directly interacts with the Li surface atoms. The binding energy of water on $Li_{0.5}CoO_{1.875}$ and $Li_{0.5}CoO_{1.75}$ for (110) and (012) terminations has not been calculated since these configurations with oxygen vacancies are higher in energy than $Li_{0.5}CoO_2$. In summary, independently of the surface termination, as higher is the Li concentration, weaker and/or more repulsive is the interaction of the surface with water molecules. Specially, to avoid the O–Li bond favors the water-surface interaction.

Focusing on the OER mechanism, the stoichiometry of $LiCoO_2$ is variable since the Li content will change as the applied voltage varies. The amount of Li directly depends on the applied potential. Therefore, it is possible that the predicted potential required to fully complete the four electron-proton transfers will be larger than the delithiation potential, being the amount of Li of the cathode at the end of the reaction different than the initial Li-content on the surface at the beginning. In

Research Article
doi.org/10.1002/batt.202300452
Chemistry Europe
European Chemical Societies Publishing

Table 1. Binding Gibbs energies (eV) and sketches of water molecule adsorbed on Li_xCoO_{2-y}. Green, blue, red, and white balls depict Li, Co, O, and H atoms respectively.

Surface	$LiCoO_2$	$Li_{0.75}CoO_2$	$Li_{0.5}CoO_2$	$Li_{0.5}CoO_{1.875}$	$Li_{0.5}CoO_{1.75}$
(001)	0.22	−0.84	−1.64	−0.89	−0.94
	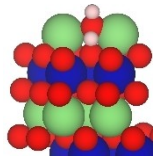	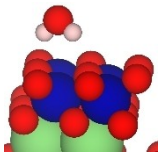	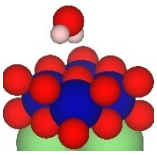	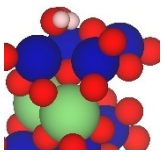	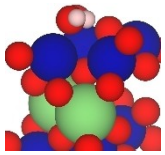
(104)	1.40	0.89	0.79	−0.33	1.11
	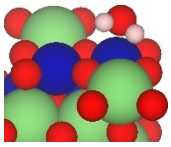	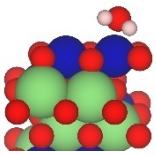	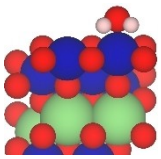	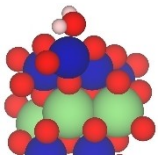	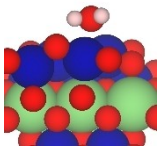
(110)	0.66	0.00	0.00	–	–
	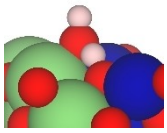	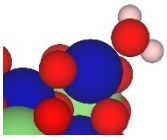	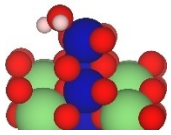		
(012)	0.94	0.80	0.28	–	–
	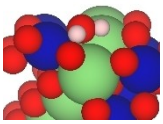	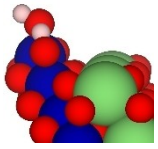	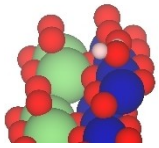		

other words, if the delithiation process occurs at lower voltages than the limiting potential, the OER will not occur at this Li concentration. It may happen specially on configurations with high Li content as it was predicted for the $LiMn_2O_4$ cathode material.[56]

Table 2 collects the delithiation voltage and limiting potentials required to produce OER [Equations (2)–(5)] and LOER [Equations (6)–(9)]. Table 2 reported as well the predicted overpotential, i.e., the difference between the limiting potential and the equilibrium potential (1.23 V). Note that the overpotential always corresponds to the step with large energy barrier of the Gibbs energy reaction pathway at 1.23 V. This step is highlighted as well in Table 2. In addition, Table S2 collects all the energy and entropic contributions for all the computed reaction mechanisms.

As depicted in Figure S3, the limiting potential (OER) for full lithiated (001) termination is 2.38 V (5.43 vs. Li^+/Li), which is not reached during the battery operation conditions since it will imply the full delithiation of the cathode. The limiting potential is even larger considering the LOER mechanism, being the O_2 generation the rate limiting step after the second proton-electron transfer, i.e., the O_2 formation. It can be unexpected the capability of full lithiated configuration to decompose the first water molecule invoking the hydroxyl moiety formation. This process is exergonic even at 0 V, although according to our DFT simulations, the $LiCoO_2 \rightarrow Li_{0.75}CoO_2$ process is still more favored than water decomposition to hydroxyl (see Table 2). Although, for the $Li_{0.75}CoO_2$ slab model, the LOER mechanism revealed the possible O_2 generation (second proton-electron transfer, see Figure S4) at equilibrium potential, once again the delithiation process for this surface occurs at voltages lower than 1.23 V (0.80 V vs. H^+/H_2), and therefore, the Li loss would arise before.

Regarding $Li_{0.5}CoO_2$ configuration, as illustrated in Figure 1(a), the rate limiting step of the OER pathway is precisely the *OH generation. Note that at equilibrium potential, all the reaction steps are energetically favored except the first one. It can be observed that LOER mechanism demands the same energy for the first proton-electron transfer since the *OH moiety is bonded to one of the O-surface atoms. For LOER path, the rate limiting step is the proton removal, since the thermodynamic barrier of this step 1.61 eV is larger than the water decomposition to *OH (0.94 eV). Anyhow, for (001) termination, the calculated overpotentials are very large independently of the reaction mechanism and the OER/LOER will not occur *a priori*. It must be kept in mind that hydroxyl generation, step I, blocks the reaction, since the subsequent steps are exergonic. Thus, it can be hypothesized that hydroxyl sources can avoid the need to overcome the energetics of the first proton-electron transfer and favor the formation of O_2 gas

Research Article
doi.org/10.1002/batt.202300452
Chemistry Europe
European Chemical Societies Publishing

Table 2. Limiting potential vs. H^+/H_2 (vs. Li^+/Li in brackets) required for surface delithiation, OER, and LOER reactions and the overpotential (V) The rate limiting step (RLS) of each surface is indicated for both OER and LOER.

Plane	Surface	Delithiation voltage [V]	OER voltage [V]	Overpotential [V]	RLS	LOER voltage [V]	Overpotential [V]	RLS
(001)	$LiCoO_2$	<-1.00 (< 2.00)	2.38 (5.43)	1.15	*O→*OOH	2.67 (5.72)		*OH→O_2(g)
	$Li_{0.75}CoO_2$	0.80 (3.85)	2.38 (5.43)	1.15	*O→*OOH	3.85 (6.90)		*H→*
	$Li_{0.5}CoO_2$	–	2.17 (5.22)	0.94	H_2O(g)→*OH	2.84 (5.89)		*H→*
	$Li_{0.5}CoO_{1.875}$	–	3.29 (5.34)	2.06	*OOH→O_2(g)	3.39 (6.44)		*OH→O_2(g)
	$Li_{0.5}CoO_{1.75}$	–	2.26 (5.31)	1.03	*OOH→O_2(g)	3.58 (6.63)		*OH→O_2(g)
(104)	$LiCoO_2$	0.17 (3.22)	2.63 (5.68)	1.40	*OH→*O	4.33 (7.38)	3.10	*OH→O_2(g)
	$Li_{0.75}CoO_2$	0.85 (3.90)	2.92 (5.97)	1.69	*OH→*O	1.79 (4.84)	0.56	H_2O(g)→*OH
	$Li_{0.5}CoO_2$	–	3.39 (6.44)	2.16	*OOH→O_2(g)	1.81 (4.86)	0.58	*H→*
	$Li_{0.5}CoO_{1.875}$	–	2.29 (5.34)	1.06	*OH→*O	2.02 (5.07)	0.79	*OH→O_2(g)
	$Li_{0.5}CoO_{1.75}$	–	2.27 (5.32)	1.04	*OH→*O	3.22 (6.27)	1.99	*OH→O_2(g)
(110)	$LiCoO_2$	−0.07 (2.98)	2.19 (5.24)	0.96	*O→*OOH	3.04 (6.09)	1.81	*OH→O_2(g)
	$Li_{0.75}CoO_2$	0.50 (3.55)	2.75 (5.80)	1.52	*OH→*O	3.14 (6.19)	1.91	*OH→O_2(g)
	$Li_{0.5}CoO_2$	–	3.08 (6.13)	1.85	H_2O(g)→*OH	3.18 (6.23)	1.95	H_2O(g)→*OH
(012)	$LiCoO_2$	0.26 (3.31)	2.20 (5.25)	0.97	*OH→*O	3.31 (6.36)	2.08	H_2O(g)→*OH
	$Li_{0.75}CoO_2$	0.54 (3.59)	2.84 (5.89)	1.61	H_2O(g)→*OH	2.84 (5.89)	1.61	H_2O(g)→*OH
	$Li_{0.5}CoO_2$	–	3.27 (6.32)	2.04	H_2O(g)→*OH	3.27 (6.32)	2.04	H_2O(g)→*OH

in the cell, since both steps are exergonic after surpassing the first water decomposition.

On the other hand, previous DFT calculations reported that the formation of oxygen vacancies and subsequent slab reconstruction stabilize the (001) termination at half Li concentration.[42] Thus, we have investigated as well both OER and LOER mechanisms considering slab models of half delithiated (001) surface including the oxygen vacancies. Figure 1(b) and (c) exhibits the (electro)catalytic pathway of OER on the $Li_{0.5}CoO_{1.875}$ and $Li_{0.5}CoO_{1.75}$ systems, showing that the overpotential required drastically increases with respect to the configuration without oxygen vacancies (Figure 1a), especially for $Li_{0.5}CoO_{1.875}$ configuration. In contrast, the presence of oxygen vacancies (electro)catalyzes the *OH formation at equilibrium potential, behaving as a potential hydroxyl source. Therefore, at equilibrium potential, the unfavored hydroxyl generation on $Li_{0.5}CoO_2$ (001) is favored on $Li_{0.5}CoO_{2-x}$ (001) and the unfavored O_2 formation on $Li_{0.5}CoO_{2-x}$ (001) (step IV for OER and II for LOER) is feasible on $Li_{0.5}CoO_2$ (001). According to our DFT data, one can hypothesize that the formation of oxygen vacancies on (001) are detrimental for the battery performance since they can behave as a hydroxyl source that facilitates the subsequent reaction steps of OER and LOER on surface regions without lattice oxygen vacancies. To make this process feasible, it should be presumed that the formation of O_{vac} is not homogeneous on the exposed surface of the material, i.e., the presence of regions with and without vacancies and the hydroxyl diffusion from one to another is mandatory. The formation of O_{vac} exhibits enhanced thermodynamic stability,[42] rendering them the predominant and inherently prevalent exposed facets within the material. Focusing on the configuration with the lowest energy surface, $Li_{0.5}CoO_{1.75}$ exhibits a very large overpotential for both OER and LOER mechanisms avoiding the O_2 generation. However, the water decomposition to *OH, *O, and *OOH species is energetically favored following the OER mechanism. The second proton-electron transfer of OER, the *O formation, can be overtaken at 0.34 V beyond the equilibrium potential (at 4.61 V vs. Li^+/Li). In addition, the third step (*OOH) is as well feasible, since this process is exergonic. Therefore, analyzing the different reaction landscapes obtained for (001) terminations, one can affirm that only half delithiated surface can play a role on OER and LOER. It is expected that the formation of oxygen vacancies helps the generation of *OH, *O, and *OOH moieties with an overpotential of 0.34 V for OER mechanism. Although no O_2 gas is produced, the water decomposition towards these moieties is not positive for the electrolyte stability since the cathode is able to decompose the electrolyte. On the other hand, the LOER mechanism studied using $Li_{0.5}CoO_{1.75}$ and $Li_{0.5}CoO_{1.875}$ (001) models revealed that the O_{vac} and O_2 generation is only possible at very large overpotentials, discarding that lattice oxygen contributes to OER.

Research Article
doi.org/10.1002/batt.202300452
Chemistry Europe
European Chemical Societies Publishing

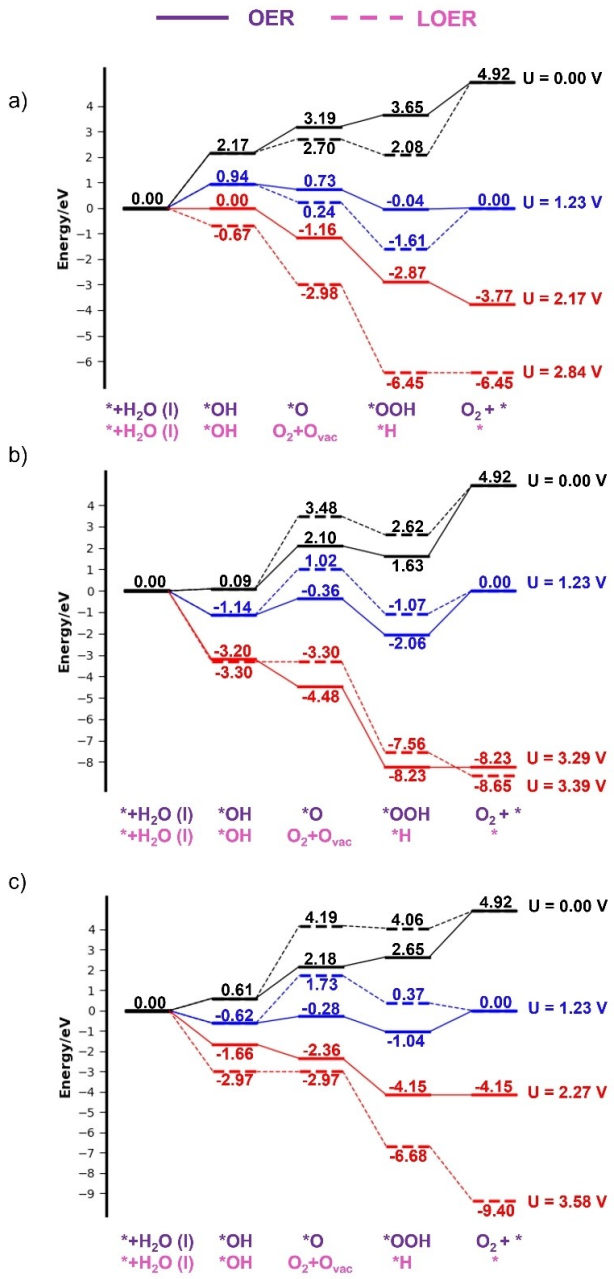

Figure 1. Gibbs energy reaction pathways for OER (purple, solid lines) and LOER (magenta, dashed lines) catalyzed by a) $Li_{0.5}CoO_2$, b) $Li_{0.5}CoO_{1.875}$, and c) $Li_{0.5}CoO_{1.75}$ (001) termination. The Gibbs energy diagram is computed at 0 V (black lines), the equilibrium potential, 1.23 V (blue lines), and the predicted limiting potential (red lines).

It is important to remark that the anchoring of hydroxyl groups on the surface of the cathode may not be detrimental *per se*. In fact, the hydroxyl coverage can help to reduce the catalytic activity of the cathode towards OER, as observed for $LiMn_2O_4$.[56] Nevertheless, the hydroxyl ions come from the water molecules of the electrolyte, and it depleted the concentration of the aqueous electrolyte in the battery. Aqueous batteries rely on the mobility of ions in the electrolyte for charge transport between the electrodes. Reduced electrolyte concentration can hinder ion mobility, leading to increased internal resistance and decreased overall battery efficiency. In addition, is expected that side reactions with hydroxide groups strongly corrode the surface of the electrodes,[57] which can lead to the degradation of electrode performance over time, reducing the overall capacity and efficiency of the battery.

Regarding the (104) cut, Figures S5 and S6 illustrate the reaction pathway for surfaces with high Li content and Figure 2 shows the Gibbs energy diagram for $Li_{0.5}CoO_{2-x}$, considering the oxygen vacancy formation according to previous surface energy studies.[42] For the full lithiated configuration, the first water

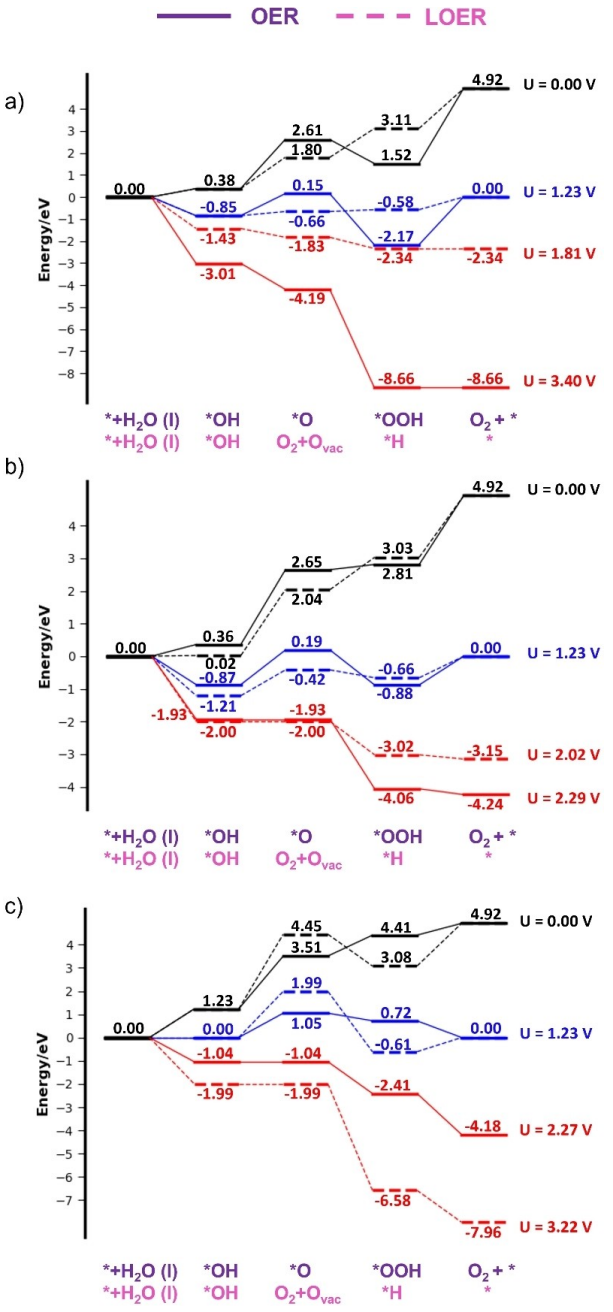

Figure 2. Gibbs energy reaction pathways for OER (purple, solid lines) and LOER (magenta, dashed lines) catalyzed by a) $Li_{0.5}CoO_2$, b) $Li_{0.5}CoO_{1.875}$, and c) $Li_{0.5}CoO_{1.75}$ (104) termination. The Gibbs energy diagram is computed at 0 V (black lines), the equilibrium potential, 1.23 V (blue lines), and the predicted limiting potential (red lines).

Research Article
doi.org/10.1002/batt.202300452
Chemistry Europe
European Chemical Societies Publishing

dissociation is feasible at equilibrium potential. The difference between OER and LOER is related to the adsorption site of hydroxyl moiety, being the binding energy on the Co site slightly favored than at the O site. In fact, the hydroxyl generation is energetically favored at 0.65 V (3.70 V vs. Li^+/Li) although the delithiation process from $LiCoO_2$ to $Li_{0.75}CoO_2$ is calculated at slightly lower voltage (see Table 2). The OER on $Li_{0.75}CoO_2$ presents a very large limiting potential, with the *OH dissociation being the rate limiting step (Figure S6).

Regarding to $Li_{0.5}CoO_2$ configuration (Figure 2a), the first water dissociation can occur at equilibrium potential. Nevertheless, at this Li content the formation of oxygen vacancies was predicted to be favored, being the predominant exposed surface at this Li concentration. Figure 2(b) and (c) illustrate that both $Li_{0.5}CoO_{1.875}$ and $Li_{0.5}CoO_{1.75}$ (104) configurations show the same tendency for OER mechanism. The first step is feasible at equilibrium potential (1.23 V) and both surfaces have the same rate limiting step for OER mechanism, the *O generation. Thereupon, our simulations discard the (104) termination as an effective and active catalysts for the electrocatalytic OER, which is excellent from the point of view of the aqueous Li-ion battery performance. Nevertheless, as observed for the (001) termination, the conversion of water molecule to an adsorbed hydroxyl moiety is feasible. Regarding the Gibbs energy landscapes for LOER, the conclusion that can be gathered is that the formation of vacancies can avoid the O_2 gas generation. Note that for the model without oxygen vacancies (Figure 2a), the difference between first and second proton transfer steady states is only 0.19 eV, which indicates that the participation of oxygen lattice reduces the required potential to produce O_2, the second proton-electron transfer, to only 1.42 V (4.46 V vs Li^+/Li). However, the involvement of the oxygen lattice on the surface with O_{vac} does not facilitate the formation of O_2 gas since an overpotential of 1.99 V is predicted for the lowest surface configuration ($Li_{0.5}CoO_{1.75}$).

Finally, we briefly discuss the (electro)catalytic activity of the higher energy terminations (110) and (012) of LCO. The no participation of oxygen lattice implies very large overpotentials independently of the Li amount (see Figures S7–S10). In addition, the vacancy generation is not energetically favored for both terminations.[42] Nevertheless, the involvement of lattice oxygen gains importance for $Li_{0.5}CoO_2$ configurations for both surface terminations (see Figure 3). Although both landscapes show that the rate limiting step is the first proton-electron transfer, this impediment may be overcome since other surface terminations can decompose water to hydroxyl moieties at equilibrium potential -for instance, $Li_{0.5}CoO_{1.75}$ (001) and $Li_{0.5}CoO_{1.75}$ (104)-. Hypothesizing that these surface terminations work as hydroxyl reservoirs, (012) and (110) terminations may skip the first proton coupled electron transfer, surpassing the rate limiting step of LOER for these surfaces. For the (110) termination, the second, third, and fourth reaction steps are thermodynamically favored. For the case of (012), a small overpotential is required to overcome the *OOH generation and to fully complete the LOER mechanism. Nevertheless, it must be considered that both terminations are higher in energy with respect (001) and (104), which will be the most exposed surfaces on the material.

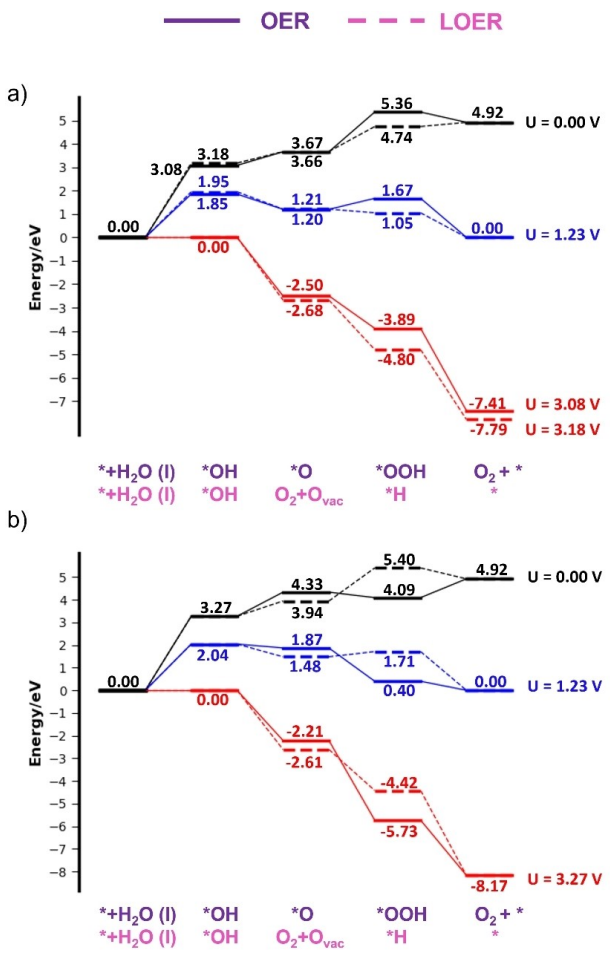

Figure 3. Gibbs energy reaction pathways for OER (purple, solid lines) and LOER (magenta, dashed lines) catalyzed by a) $Li_{0.5}CoO_2$ (110) and b) $Li_{0.5}CoO_2$ (012) termination. The Gibbs energy diagram is computed at 0 V (black lines), the equilibrium potential, 1.23 V (blue lines), and the predicted limiting potential (red lines).

Conclusions

In this work, DFT calculations have been carried out to unveil the oxygen evolution reaction mechanism on $LiCoO_2$, the most common cathode material adopted in Li-ion batteries, with the goal to substitute the common organic electrolytes by water. The well-known four proton-electron transfer oxygen evolution reaction (OER) mechanism has been evaluated as well as the role of the lattice oxygen on the OER and lattice OER (LOER). The polar (001) and (012) terminations and the non-polar (104) and (110) surfaces have been investigated since they are the lowest in energy terminations.

The binding energy of the water molecule has been computed, showing that as much Li content on the surface, a weaker and even repulsive adsorption is found, in agreement with the experimental evidence. Regarding the OER and LOER Gibbs energy diagrams, three main conclusions are achieved:

firstly, large Li concentrations on the surface does not promote OER and LOER, since the delithiation process occurs at lower potentials. Secondly, the participation of oxygen lattice on oxygen evolution depends on the surface cut and surface stoichiometry, i.e., in some cases oxygen lattice decreases the required overpotential for OER. Last but not least, DFT simulations predict (except for one particular configuration) very large overpotentials for O_2 generation, which cannot be reached during battery operation conditions. Nevertheless, these large overpotentials does not imply the stability of the electrolyte, since water decomposition is predicted. For instance, the first proton-electron transfer is exergonic at equilibrium potential for $Li_{0.5}CoO_{1.75}$ and $Li_{0.5}CoO_{1.875}$ (001) and for all configurations of half delithiated surfaces of (104), with and without oxygen vacancies. Therefore, water is decomposed to hydroxide. Moreover, it is predicted the water decomposition towards *OH, *O, and *OOH on half delithiated surfaces of (104) with a very small overpotential, which show that the partial water decomposition occurs. Thus, focusing conclusions exclusively on the potential required for O_2 gas production is not accurate, since partial water decomposition reactions are as well bad for the electrolyte stability and the subsequent battery performance.

In summary, the formation of O_2 gas is not expected according to DFT simulations on the lowest energy LCO surface terminations at the voltage window commonly applied during battery operations using aqueous electrolytes. It is predicted the first proton-electron process at equilibrium potential ($H_2O(l) + * \rightarrow *OH + H^+ + e^-$) in the lowest energy surface terminations, (001) and (104), and it has been revealed the role of the oxygen vacancies on the material, stabilizing the half delithiated configurations and increasing the overpotential for the formation of gaseous O_2. Our DFT study highlights LCO not as a O_2 gas promotor, but presents the drawbacks of water decomposition to hydroxyl, which may provoke the formation of cobalt and lithium hydroxides at the interface.

Author Contributions

Gibu George: Investigation, Data Curation, Visualization, Writing-review & editing; Albert Poater: Formal analysis, Supervision, Funding acquisition, Resources, Writing-review & editing; Miquel Solà: Formal analysis, Supervision, Funding acquisition, Resources, Writing-review & editing; Sergio Posada-Pérez: Conceptualization, Data Curation, Formal Analysis, Supervision, Funding acquisition, Investigation, Methodology, Writing-original draft.

Acknowledgements

S.P.-P. appreciates the economic support of Marie Curie fellowship (H2020-MSCA-IF-2020-101020330). A.P. is a Serra Húnter Fellow and received the ICREA Academia Prize 2019. M.S. and A.P. thank the Spanish MINECO for projects PID2020-13711GB-I00 and PGC2018-097722-B-I00, and the Generalitat de Catalunya for project 2021SGR623. Computational time at the MARENOSTRUM supercomputer has been provided by the Barcelona Supercomputing Centre through a grant from Red Española de Supercomputación, project (QHS-2022-3-0002). Open access funding provided by Universitat de Girona.

Conflict of Interests

The authors have no conflict of interest to declare.

Data Availability Statement

The data that support the findings of this study are available from the corresponding author upon reasonable request.

Keywords: aqueous li-ion batteries · energy storage · lithium cobalt oxide · lattice oxygen evolution reaction · density functional calculations

[1] K. Mizushima, P. C. Jones, P. J. Wiseman, J. B. Goodenough, *Mater. Res. Bull.* **1980**, *15*, 783–789.
[2] J. Molenda, A. Stokłosa, *Solid State Ion* **1989**, *36*, 53–58.
[3] A. Yoshino, *Angew. Chem. Int. Ed.* **2012**, *51*, 5798–5800.
[4] R. Yazami, P. Touzain, *J. Power Sources* **1983**, *9*, 365–371.
[5] W. Li, J. R. Dahn, D. S. Wainwright, *Science* **1994**, *264*, 1115–1118.
[6] Z. Chang, C. Li, Y. Wang, B. Chen, L. Fu, Y. Zhu, L. Zhang, Y. Wu, W. Huang, *Sci. Rep.* **2016**, *6*, 2–7.
[7] L. Smith, B. Dunn, *Science* **2015**, *350*, 918.
[8] H. Kim, J. Hong, K. Y. Park, H. Kim, S. W. Kim, K. Kang, *Chem. Rev.* **2014**, *114*, 11788–11827.
[9] D. H. Doughty, P. C. Butler, A. A. Akhil, N. H. Clark, J. D. Boyes, *Electrochem. Soc. Interface* **2010**, *19*, 49–53.
[10] S. Chen, S. R. Jeong, S. Tao, *Mater. Rep. Energy* **2022**, *2*, 100096.
[11] A. von Wald Cresce, K. Xu, *Carbon Energy* **2021**, *3*, 721–751.
[12] H. Zhang, X. Liu, H. Li, I. Hasa, S. Passerini, *Angew. Chem. Int. Ed.* **2021**, *60*, 598–616.
[13] X. Zhu, M. Mao, Z. Lin, J. Yue, M. Li, T. Lv, A. Zhou, Y.-S. Hu, H. Li, X. Huang, L. Chen, L. Suo, *ACS Materials Lett.* **2022**, *4*, 1574–1583.
[14] M. H. Lee, S. J. Kim, D. Chang, J. Kim, S. Moon, K. Oh, K.-Y. Park, W. M. Seong, H. Park, G. Kwon, B. Lee, K. Kang, *Mater. Today* **2019**, *29*, 26–36.
[15] Q. Ni, B. Kim, C. Wu, K. Kang, *Adv. Mater.* **2022**, *34*, 2108206.
[16] J. Choi, E. Alvarez, T. A. Arunkumar, A. Manthiram, *Electrochem. Solid-State Lett.* **2006**, *9*, A241.
[17] R. Benedek, M. M. Thackeray, A. van de Walle, *Chem. Mater.* **2008**, *20*, 5485–5490.
[18] H. Tomiyasu, H. Shikata, K. Takao, N. Asanuma, S. Taruta, Y. Y. Park, *Sci. Rep.* **2017**, *7*, 1–12.
[19] F. Wan, J. Zhu, S. Huang, Z. Niu, *Batteries & Supercaps* **2020**, *3*, 323–330.
[20] J. O. G. Posada, A. J. R. Rennie, S. P. Villar, V. L. Martins, J. Marinaccio, A. Barnes, C. F. Glover, D. A. Worsley, P. J. Hall, *Renew. Sust. Energ. Rev.* **2017**, *68*, 1174–1182.
[21] J. Qian, L. Liu, J. Yang, S. Li, X. Wang, H. L. Zhuang, Y. Lu, *Nat. Commun.* **2018**, *9*, 4918.
[22] Q. Liu, X. Su, D. Lei, Y. Qin, J. Wen, Y. A. Wu, Y. Rong, R. Kou, X. Xiao, F. Aguesse, J. Bareño, Y. Ren, W. Lu, Y. Li, *Nat. Energy* **2018**, *3*, 936–943.
[23] Y. Ji, J. Wei, D. Liang, B. Chen, X. Li, H. Zhang, Z. Yin, *Nanoscale* **2023**, *15*, 11898–119.
[24] Z. Zhuang, J. Wang, K. Jia, G. Ji, J. Ma, Z. Han, Z. Piao, R. Gao, H. Ji, X. Zhong, G. Zhou, H.-M. Cheng, *Adv. Mater.* **2023**, *35*, 2212059.
[25] S. Xu, X. Tan, W. Ding, W. Ren, Q. Zhao, W. Huang, J. Liu, R. Qi, Y. Zhang, J. Yang, C. Zuo, H. Ji, H. Ren, B. Cao, H. Xue, Z. Gao, H. Yi, W. Zhao, Y. Xiao, Q. Zhao, M. Zhang, F. Pan, *Angew. Chem. Int. Ed.* **2023**, *62*, e202218595; *Angew. Chem.* **2023**, *135*, e202218595.
[26] J. Fernández-Rodriguez, L. Hernan, J. Morales, J. Tirado, *Mater. Res. Bull.* **1988**, *23*, 899–904.

[27] S. Posada-Pérez, G. M. Rignanese, G. Hautier, *Chem. Mater.* **2021**, *33*, 6942–6954.
[28] R. Ruffo, C. Wessells, R. A. Huggins, Y. Cui, *Electrochem. Commun.* **2009**, *11*, 247–249.
[29] W. Tang, L. L. Liu, S. Tian, L. Li, Y. B. Yue, Y. P. Wu, S. Y. Guan, K. Zhu, *Electrochem. Commun.* **2010**, *12*, 1524–1526.
[30] A. Ramanujapuram, D. Gordon, A. Magasinski, B. Ward, N. Nitta, C. Huang, G. Yushin, *Energy Environ. Sci.* **2016**, *9*, 1841–1848.
[31] J. Jin, Y. Liu, J. Chen, *Batteries & Supercaps* **2023**, *6*, e202300347.
[32] F. Wang, Y. Lin, L. Suo, X. Fan, T. Gao, C. Yang, F. Han, Y. Qi, K. Xu, C. Wang, *Energy Environ. Sci.* **2016**, *9*, 3666–3673.
[33] X. Huang, J. W. Bennett, M. N. Hang, E. D. Laudadio, R. Hamers, S. E. Mason, *J. Phys. Chem. C* **2017**, *121*, 5069–5080.
[34] A. Abbaspour-tamijani, J. W. Bennett, D. T. Jones, Z. R. Jones, E. D. Laudadio, J. Robert, J. A. Santana, S. E. Mason, *Appl. Surf. Sci.* **2020**, *515*, 145865.
[35] G. Kresse, J. Furthmüller, *Phys. Rev. B: Condens. Matter Mater. Phys.* **1996**, *54*, 11169.
[36] J. P. Perdew, K. Burke, M. Ernzerhof, *Phys. Rev. Lett.* **1996**, *77*, 3865.
[37] S. Dudarev, G. Botton, *Phys. Rev. B: Condens. Matter Mater. Phys.* **1998**, *57*, 1505.
[38] A. Jain, S. P. Ong, G. Hautier, W. Chen, W. D. Richards, S. Dacek, S. Cholia, D. Gunter, D. Skinner, G. Ceder, K. A. Persson, *APL Mater.* **2013**, *1*, 011002.
[39] P. E. Blöchl, *Phys. Rev. B* **1994**, *50*, 17953–17979.
[40] D. Joubert, *Phys. Rev. B: Condens. Matter Mater. Phys.* **1999**, *59*, 1758–1775.
[41] J. D. Pack, H. J. Monkhorst, *Phys. Rev. B* **1977**, *16*, 1748–1749.
[42] S. Posada-Pérez, G. Hautier, G. M. Rignanese, *J. Phys. Chem. C* **2022**, *126*, 110–119.
[43] D. Kramer, G. Ceder, *Chem. Mater.* **2009**, *21*, 3799–3809.
[44] A. Moradabadi, P. Kaghazchi, *Phys. Chem. Chem. Phys.* **2015**, *17*, 22917–22922.
[45] L. Hong, L. Hu, J. W. Freeland, J. Cabana, S. Ögüt, R. F. Klie, *J. Phys. Chem. C* **2019**, *123*, 8851–8858.
[46] P. W. Tasker, *J. Phys. C: Solid State Phys.* **1979**, *12*, 4977–4984.
[47] I. C. Man, H. Y. Su, F. Calle-Vallejo, H. A. Hansen, J. I. Martínez, N. G. Inoglu, J. Kitchin, T. F. Jaramillo, J. K. Nørskov, J. Rossmeisl, *ChemCatChem* **2011**, *3*, 1159–1165.
[48] J. A. Luque-Urrutia, T. Ortiz-García, M. Solà, A. Poater, *Inorganics* **2023**, *11*, 88.
[49] J. S. Yoo, X. Rong, Y. Liu, A. M. Kolpak, *ACS Catal.* **2018**, *8*, 4628–4636.
[50] K. S. Exner, *ChemCatChem* **2021**, *13*, 4066–4074.
[51] E. Fabbri, T. J. Schmidt, *ACS Catal.* **2018**, *8*, 9765–9774.
[52] A. Zagalskaya, I. Evazzade, V. Alexandrov, *ACS Energy Lett.* **2021**, *6*, 1124–1133.
[53] J. K. Nørskov, J. Rossmeisl, A. Logadottir, L. Lindqvist, J. R. Kitchin, T. Bligaard, H. Jónsson, *J. Phys. Chem. B* **2004**, *108*, 17886–17892.
[54] P. S. Maram, G. C. C. Costa, A. Navrotsky, *Angew. Chem. Int. Ed.* **2013**, *52*, 12139–12142.
[55] G. Cherkashinin, W. Jaegermann, *J. Chem. Phys.* **2016**, *144*, 219901.
[56] G. George, S. Posada-Pérez, A. Poater, M. Solà, *Appl. Surf. Sci.* **2023**, *612*, 155822.
[57] H. Zhang, X. Liu, H. Li, I. Hasa, S. Passerini, *Angew. Chem. Int. Ed.* **2021**, *60*, 598.

Manuscript received: October 5, 2023
Revised manuscript received: November 26, 2023
Accepted manuscript online: November 29, 2023
Version of record online: December 15, 2023